An investigation of the relationship between tropical monsoon precipitation changes and stratospheric sulfate aerosol optical depth

Oxford Open Climate Change, 2024, **4(1),** kgae016
https://doi.org/10.1093/oxfclm/kgae016
Advance Access Publication Date: 21 August 2024
Research Article

An investigation of the relationship between tropical monsoon precipitation changes and stratospheric sulfate aerosol optical depth

Anu Xavier [1,*], Govindasamy Bala[1], Shinto Roose[2], Usha KH[1,3]

[1]Centre for Atmospheric and Oceanic Sciences, Indian Institute of Science, Bangalore 560012, India
[2]Department of Civil Engineering, McGill University, Montreal, QC, H3A 0C3, Canada
[3]Present address: Atria University, ASKB Campus, Anandnagar, Bengaluru 560 024, India

*Corresponding author. Centre for Atmospheric and Oceanic Sciences, Indian Institute of Science, Bangalore 560012, India. E-mail: anuxavier26@gmail.com

Abstract

Stratospheric aerosol geoengineering (SAG) is one of the several solar geoengineering options that have been proposed to counteract climate change. In the case of SAG, reflective aerosols injected into the stratosphere would reflect more sunlight and cool the planet. When assessing the potential efficacy and risks of SAG, the sensitivity of tropical monsoon precipitation changes should be also considered. Using a climate model, we perform several stylized simulations with different meridional distributions and amounts of volcanic sulfate aerosols in the stratosphere. Because tropical monsoon precipitation responds to global mean and interhemispheric difference in radiative forcing or temperature, we quantify the sensitivity of tropical monsoon precipitation to SAG in terms of two parameters: global mean aerosol optical depth (GMAOD) and interhemispheric AOD difference (IHAODD). For instance, we find that the simulated northern hemisphere monsoon precipitation has a sensitivity of $-1.33 \pm 0.95\%$ per 0.1 increase in GMAOD and $-7.62 \pm 0.27\%$ per 0.1 increase in IHAODD. Our estimated precipitation changes in terms of the two sensitivity parameters for the global mean precipitation and for the indices of tropical, northern hemisphere, southern hemisphere and Indian summer monsoon precipitation are in good agreement with the model simulated precipitation changes. Similar sensitivity estimates are also made for unit changes in global mean and interhemispheric differences in effective radiative forcing and surface temperature. Our study based on planetary energetics provides a simpler framework for understanding the tropical monsoon precipitation response to external forcing agents.

Keywords: Stratospheric aerosol geoengineering (SAG); tropical monsoon; global mean aerosol optical depth (GMAOD); interhemispheric aerosol optical depth difference (IHAODD); effective radiative forcing (ERF); Indian summer monsoon

Introduction

The global mean surface temperature is 1.1°C higher in the recent decade (2011–2020) than the preindustrial period (1850–1900) primarily because of anthropogenic greenhouse gas emissions. [1, 2]. The consequences of this increase in temperature are experienced across the globe. It ranges from melting glaciers, increase in sea level rise, shifts in precipitation patterns to increase in temperature and precipitation extremes. Further, these consequences pose significant risk to human health, agriculture, biodiversity, and overall global and regional economy [2, 3]. The actions taken to achieve the Paris Agreement's temperature targets in limiting global warming to below 1.5°C are deemed insufficient [4–8]. Consequently, to counteract some of the adverse effects of global warming, a suite of solar geoengineering approaches has been proposed [9–13].

Geoengineering' refers to deliberate planetary scale intervention to combat climate change impacts [14, 15]. It includes Carbon dioxide removal (CDR) and solar geoengineering, also known as solar radiation modification (SRM) [2, 16]. SRM is relatively a cheap but an imperfect option when compared to adaptation and mitigation [10, 17–20]. Three aerosol-based SRM options have recently gained attention: stratospheric aerosol injection, marine cloud brightening and cirrus cloud thinning [11, 21–25].

The most studied SRM option involves the injection of sulfate aerosols into the stratosphere, commonly referred to as stratospheric aerosol geoengineering (SAG). As sulfate aerosols are highly reflective, they cause negative radiative forcing which can partly or completely offset the positive radiative forcing from greenhouse gases. The radiative forcing of the sulfate aerosols depends on the altitude, latitude, season of injection as well as the size distribution of the aerosols [26–33].

Despite SAG being considered as one of the more viable SRM options, climate modeling studies have raised concerns about its potential negative impacts on the global and regional hydrology [5, 19, 34–37]. SAG could also change the ozone concentration in the stratosphere [38–42], affect human health and have ecological impacts [43–45]. Additionally, significant uncertainties surround the climate response to the factors such as the injection latitude, altitude, and the overall distribution of aerosols, as highlighted by [15, 31, 46, 47]. Terminating SRM abruptly would lead to an abrupt temperature and precipitation changes, with rates 5–20 times larger than those associated with current

Received: January 12, 2024. **Revised:** April 19, 2024. **Accepted:** August 07, 2024

gradual global warming. This is commonly referred to as the "termination effect" [5, 48–50].

The changes in tropical monsoon precipitation in a changing climate is an important issue from both scientific and societal perspectives as monsoons characterize the fundamental aspects of the tropical climate [51, 52]. About 56% of total global rainfall occurs over Tropics [53] and the rainfall intensity over tropical monsoon regions are expected to increase under the warming climate [54, 55]. In SRM simulations, however, global hydrological cycle is shown to slow down when global mean warming is completely offset [34, 36, 56, 57]. SRM would also influence regional precipitation, with large impact on tropical monsoon including Indian summer monsoon [32, 34, 35, 58–60]. Modeling studies have shown that the negative radiative forcing due to sulfate SAG could lead to planetary cooling and a reduction in tropical monsoon precipitation [32, 61]. Further, [32] showed that the interhemispheric AOD differences (IHAODD) created by injecting aerosols at single latitudes could lead to latitudinal shifts in the ITCZ. This in turn could result in tropical monsoon precipitation changes. [60] As the latitudinal position of ITCZ is a function of interhemispheric temperature differences, several studies have quantified the shift in ITCZ (and in turn the tropical monsoon precipitations) in terms of the interhemispheric temperature differences [32, 47, 62] or interhemispheric tropical temperature differences [63]. As discussed in [60], this relation is only an "association" since the changes in both interhemispheric temperature differences and ITCZ shifts represent the response to the introduced climate forcing. Therefore, using stylized meridional distribution of volcanic sulfate aerosols in the stratosphere, [60] quantified the sensitivity of tropical monsoon precipitation in the terms of IHAODD, one of the "causes". The objective of this study is, as a sequel to [60], to develop a framework which relates two "causes" (interhemispheric difference in AOD and global mean AOD) to the "effect" (tropical monsoon precipitation changes), in the specific case of stratospheric aerosol geoengineering.[60].

Even with no IHAODD, precipitation was found to decrease in the tropical monsoon regions in [60]. Though this aspect was not further explored in [60], it was suggested that the reduction in precipitation could be due to global mean AOD (GMAOD) increase. Thus, although [32] and [60] identified and quantified the influence of IHAODD on tropical monsoon precipitation, a simple framework to characterize the tropical precipitation for SAG is still lacking. In this paper, we propose a simple framework based on planetary energetics to explain the tropical monsoon precipitation change for SAG. Under this framework, we characterize the tropical precipitation changes in terms of just two independent AOD parameters: global mean AOD (GMAOD) and interhemispheric AOD difference (IHAODD) The proposed estimation can be represented by the following equation:

$$\Delta P\ (\%) = a\left(\frac{AOD_N + AOD_S}{2}\right) + b(AOD_N - AOD_S) + r \qquad (1)$$

where ΔP denotes precipitation changes in the tropical monsoon regions. The coefficients 'a' and 'b' are the sensitivity factors associated with the GMAOD and IHAODD respectively. The variables AOD_N and AOD_S represent the mean AOD in the northern hemisphere (NH) and the southern hemisphere (SH), respectively, and r is the residual. In this paper, we apply Equation (1) separately for different monsoon regions as the values of these coefficients could be different for different monsoon regions because of differences in regional geometry and regional circulations. We have proposed only two parameters in Equation (1) because our interest in this paper is primarily to characterize tropical monsoon precipitation changes. Future studies should consider additional parameters such as equator to pole AOD gradient which is likely an important driver for mid-latitude precipitation changes under SAG.

The main purpose of our study is, in the context of stratospheric aerosol geoengineering, to characterize tropical monsoon precipitation changes in terms of global mean AOD and interhemispheric differences in AOD. As AOD, effective radiative forcing (ERF) and surface temperature (TS) are all linearly related, we also characterize the monsoon precipitation changes in terms of changes in global mean ERF (TS) and interhemispheric differences in ERF (TS) by replacing AOD in Equation (1) with ERF and TS (see section "Sensitivity parameters") [60].

Data and methodology

Model description

To quantify the influence of both GMAOD and IHAODD on tropical monsoon precipitation, we use the Community Earth System model (CESM), a global climate model developed at the National Center for Atmospheric Research (NCAR), specifically version 1.0.4 [64]. Within the CESM framework, we use the Community Atmosphere Model version 4 (CAM4), with a horizontal resolution of 1.9° × 2.5° (latitude × longitude) and 26 hybrid sigma-pressure vertical layers [65, 66]. Additionally, CAM4 is coupled with a land model, the Community Land Model version 4, following the methodology described by [67]. Furthermore, sea ice is coupled to CAM4 through the Community Ice Code version 4 [68]. Our model configuration and simulation design closely resemble the approach by [60]. In the default configuration, approximately 0.6 Mt of background aerosols in the form of ammonium sulfate [47] is prescribed in the stratosphere in CAM4. In our SAG simulations, we use large volcanic sulfate aerosols that maintain a fixed fractional composition (75% sulfuric acid and 25% water). These aerosols are distributed log-normally with effective mean radius of 0.426 μm and geometric standard deviation of 1.25 [65].

Model simulations

We conducted two primary simulations: a baseline experiment referred to as '1 × CO2,' where the atmospheric CO_2 concentration is 400 ppm, and control climate change experiment called '2× CO2,' where the CO_2 concentration is doubled to 800 ppm. We performed five SAG simulations with different meridional distributions (Fig. 1a) for three different total amounts of volcanic sulfate aerosols; 25.76, 17.17 and 8.08 Mt. It may be noted that the additional stratospheric sulfate aerosols of 25.76 Mt in the Uniform case offsets the warming caused by the doubling of CO_2 (Fig. 1b). Thus, 15 SAG simulations were conducted. The aerosols in all SAG experiments are introduced to the climate state of 2× CO2 (CO_2 concentration of 800 ppm). The volcanic sulfate aerosols prescribed in the stratosphere are distributed meridionally following [15, 63, 69] and [60]. As aerosols are prescribed in this study, the aerosol microphysics, chemistry and transport are not simulated. To create the volcanic sulfate aerosol forcing, we utilized the standard CAM4 forcing file "CCSM4_volcanic_1850–2008_prototype1.nc" [70]. In each SAG experiment, 87% of the total amount is prescribed at 37 hPa (~22 km) and 13% at 23 hPa (~25 km).

The names of the SAG simulations with five different meridional distributions considered in this study are same as in [60] (Fig. 1a) and are as follows: (i) **Uniform—**Additional aerosols are uniformly distributed around the globe (Legendre polynomial of

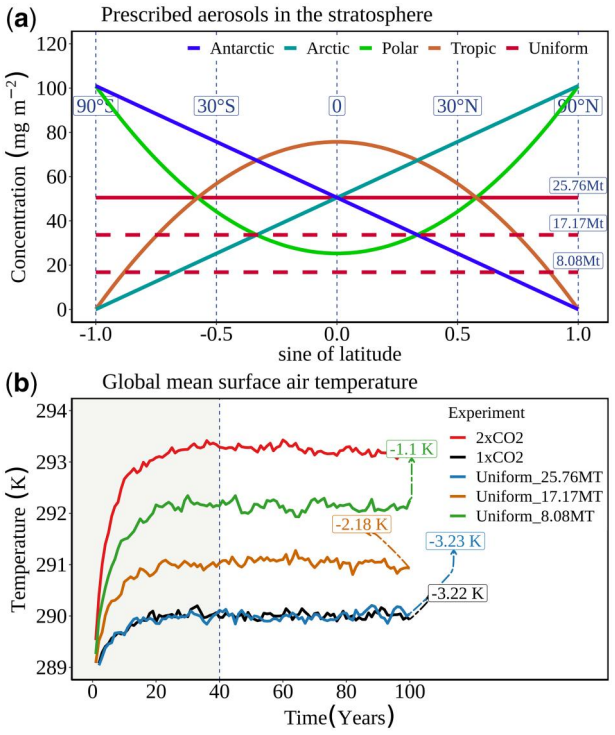

Figure 1. (a) The meridional distribution of zonal mean concentration of volcanic sulfate aerosols prescribed in the stratosphere and (b) the temporal evolution of the global-mean annual surface temperature in the 100-year slab-ocean simulations in the 1 × CO2, 2 × CO2 and the Uniform cases where the total amount of aerosols is 25.76, 17.17 and 8.08 Mt. The numbers in (b) show the global annual mean change in surface temperature in the respective experiment relative to the 2 × CO2 simulation averaged over the last 60 years (non-shaded region).

order 0; L0); (ii) **Tropic**—Aerosol concentration is parabolic with maximum at the equator (Legendre polynomial L0–L2, where L2 is Legendre polynomial of second order); (iii) **Polar**—Aerosol concentration is parabolic distribution with maximum at the poles (L0 + L2); (iv) **Arctic**—Aerosol concentration increases linearly (in sine of latitude) from south pole toward the north pole (L0 + L1); (v) **Antarctic**—Linear (in sine of latitude) increase of aerosol concentration from north pole to south pole (L0–L1).).

All 17 experiments (Table 1), including the 1× CO2, 2× CO2 and the 15 SAG simulations are performed with both prescribed SST and slab ocean configurations of the model. The last 30 years of the 60-year prescribed-SST simulations are used for the estimation of effective radiative forcing [28, 71]. The prescribed SST simulations are used only for the estimation of the ERF. In the case of slab ocean simulations, the last 60 years of the 100-year simulations are used for the analysis of climate change. In our study as in [60], equilibrium climate change is estimated in slab ocean simulations and hence climate responses are likely overestimated compared to transient simulations by fully coupled climate models.

Tropical monsoon regions

We select the tropical monsoon regions using criteria defined by [52]. As per this criteria, local summer precipitation is greater than 35% of annual precipitation in the monsoon regions and the difference between the local summer (June to August in NH and December to February in SH) and winter precipitation (DJF in NH and JJA in SH) exceeds 180 mm/year in the tropical monsoon regions. Supplementary Fig. S1 shows the tropical monsoon regions following these criteria based on our 1 × CO2 slab-ocean simulation. In this study, we have defined Northern Hemisphere Monsoon index (NHMI) and Southern Hemisphere Monsoon index (SHMI) as the mean summer precipitation in the northern and the southern hemisphere tropical regions, respectively. The Tropical monsoon index (TMI) is defined as the sum of NHMI and SHMI [32, 60]. For these three indices, analysis is solely based on summer monsoon precipitation over the land areas. In the following subsections, we examine the sensitivity of TMI, NHMI, SHMI, and the Indian summer monsoon precipitation to both GMAOD and IHAODD. Roose *et al.* [60] quantified the sensitivity of the tropical monsoons to only IHAODD with a limited number (five) of simulations, but we use 15 simulations in our analysis to quantify the sensitivity to both GMAOD and IHAODD.

Sensitivity parameters

The sensitivity parameters 'a' for GMAOD is determined from a linear regression analysis using 9 simulations with symmetric distribution of volcanic sulfate aerosols (Uniform, Tropic and Polar) for 25.76, 17.17 and 8.08 Mt of aerosols amounts. The estimation of the sensitivity parameter 'b' uses all 15 simulations with all five latitudinal distributions and for the three aerosol amounts (25.76, 17.17 and 8.08 Mt). The effect of GMAOD is removed while performing the regression with respect to IHAODD.

Since AOD, ERF and TS are linearly related to each other [60], as discussed in the Introduction, our formulation can be framed in terms of ERF and TS as well. Hence, precipitation change can also be expressed in terms of ERF and TS using equation similar to Equation (1).

$$\Delta P\ (\%) = c\left(\frac{ERF_N + ERF_S}{2}\right) + d\ (ERF_N - ERF_S) + r \quad (2)$$

$$\Delta P\ (\%) = e\left(\frac{TS_N + TS_S}{2}\right) + f\ (TS_N - TS_S) + r \quad (3)$$

where coefficients 'c', 'd', 'e' and 'f' represent sensitivity parameter for global mean ERF (GMERF), global mean TS (GMTS), interhemispheric ERF difference (IHERFD) and interhemispheric TS difference (IHTSD), respectively. The subscripts N and S denote the NH and SH mean values. The procedure for estimating the parameters in Equations (2) and (3) is similar to the procedure used for the estimation of the parameters in Equation (1). We expect that the coefficients in Equations (1–3) would be different for the different monsoon indices because of the differences in regional geometry and regional circulations between different monsoon regions.

Validation experiments

For the validation of our proposed relationships (Equations 1–3), we conducted six additional simulations (Table 1 and Supplementary Fig. S2): (i) **Arctic_L**—same as the Arctic simulation but the aerosol concentration increases linearly toward the north pole from the south pole; (ii) **Antarctic_L**—same as the Antarctic simulation but the aerosol concentration increases linearly towards the south pole from the north pole; (iii) **NHmid**—Aerosols concentration is distributed as a function of sine(2lat) with maximum at 45° N and minimum at 45° S.; (iv) **SHmid**—Similar to the NHmid case but with maximum at 45° S and minimum at 45° N; (v) **L0pL3**—Uniform aerosol distribution (L0) is added to the third order of Legendre polynomial (L3); (vi) **L0mL3**—Uniform aerosol distribution (L0) minus Legendre polynomial of the third order (L3). The aerosol distribution in these

Table 1. List of simulations

Experiment	Details
1 × CO2	CO_2 concentration 400 ppm (Baseline)
2 × CO2	CO_2 concentration 800 ppm (Control climate change)
SAG experiments	
Uniform	25.76 Mt, 17.17 Mt, 8.08 Mt of aerosols; uniform distribution
Tropic	25.76 Mt, 17.17 Mt, 8.08 Mt of aerosols; parabolic distribution with maximum at the equator
Polar	25.76 Mt, 17.17 Mt, 8.08 Mt of aerosols; parabolic distribution with maximum at the poles
Arctic	25.76 Mt, 17.17 Mt, 8.08 Mt of aerosols; increases linearly (with sine of latitude) from the south to north pole
Antarctic	25.76 Mt, 17.17 Mt, 8.08 Mt of aerosols; increases linearly (with sine of latitude) from the north to south pole
Validation	
Arctic_L	25.76 Mt of aerosols, increases linearly from the south pole to the north pole
Antarctic_L	25.76 Mt of aerosols, increases linearly from the north to the south pole
NHmid	25.76 Mt of aerosols, function of sin (2xlat) with maximum at 45° N and minimum at 45° S
SHmid	25.76 Mt of aerosols, function of sin (2xlat) with maximum at 45°S and minimum at 45°N
L0pL3	25.76 Mt of aerosols, Uniform plus Legendre polynomial of third order (L3)
L0mL3	25.76 Mt of aerosols, Uniform minus Legendre polynomial of third order (L3)

simulations were selected to ensure that they differed from the distributions in simulations that are used to determine the sensitivity parameters, in Equations (1–3).

Results

AOD, effective radiative forcing, and surface temperature

Aerosol optical depth (AOD) characterizes the aerosol concentrations and is one of the key parameters in determining the aerosol's climate impact. The spatial distributions of AOD (Supplementary Fig. S3) and surface temperature (Supplementary Fig. S6) in SAG experiments relative to the 2 × CO2 simulation show patterns similar to those in [60]. In all the SAG cases with 25.76 Mt for the total amount of aerosols, the increase in AOD relative to 2 × CO2 is 0.19. As expected, with the increasing amount of sulfate aerosols prescribed in stratosphere, the change in AOD relative to 2 × CO2 also increases but the meridional patterns remain the same (Supplementary Fig. S4).

According to the IPCC's Fifth Assessment Report (AR5) [72], the "Effective radiative forcing (ERF)" is defined as the radiative flux at the TOA after accounting for adjustments in the stratosphere, troposphere, and land surface. In this study, the ERF is estimated using two-point method following [27, 60].

Figure 2 shows the spatial pattern of ERF for the 1 × CO2 and the five stratospheric geoengineering cases with 25.76 Mt of aerosols relative to 2 × CO2. The Tropic simulation shows more negative ERF as the net solar radiation is larger in the tropics, and this result remains valid when the aerosol amounts prescribed in the stratosphere are changed (Fig. 2 and Supplementary Fig. S5; Table 2 and Supplementary Table S1). In the Arctic and Antarctic simulations, larger interhemispheric differences in ERF are simulated. For reduced amounts of sulfate aerosols prescribed, ERF follows the same pattern but with reduced magnitude (Supplementary Fig. S5).

The change in surface temperature (TS) in the 1 × CO2 simulation relative to 2 × CO2 is about –3.22 K (Supplementary Fig. S6). On introducing 25.76 Mt of volcanic sulfate aerosols in the stratosphere, the warming is almost offset in the case of Uniform distribution (Supplementary Fig. S6). The Tropic and Arctic simulations show less cooling than the Uniform simulation and the cooling is larger in the case of Polar and Antarctic simulations. For different aerosol masses, the global mean temperature changes show maximum cooling in the Polar cases whereas minimum cooling is simulated in the Tropic cases (Table 2 and Supplementary Table S1). This is consistent with the findings of [60] and [63]. The SAG cases with total aerosol mass of 25.76 Mt, 17.17 Mt and 8.08 Mt (Supplementary Fig. S7) show similar surface cooling pattern and the amount of cooling increases as the mass of aerosols increases. The larger cooling in the Polar experiment is likely due to the combined effect of local lapse-rate, ice-albedo and Planck feedback [73]. This is also consistent with the finding that a forcing in the extratropical regions leads to more global mean temperature changes than a forcing in the tropics [31, 74, 75].

Precipitation response and ITCZ shift

A reduction in global mean precipitation is expected with a decrease in the global mean temperature [76, 77]. Consistently, many solar geoengineering studies [15, 27, 34, 36, 47, 59, 60, 78, 79] have shown that the cooling produced by SAG leads to a weakening of the hydrological cycle. However, when the global mean cooling in SRM simulations exactly offsets the CO_2 induced global mean warming, an exact offset of global mean precipitation is not simulated by models, because the precipitation reduction resulting from the fast tropospheric adjustment to CO_2 radiative forcing is not offset by fast adjustment to sulfate aerosol forcing [36, 79–81].

Global mean precipitation changes relative to the 2 × CO2 simulations show a decline with the largest reduction in the Antarctic case (−8.67%) and least reduction in the Arctic case (−7.29%) with 25.76 Mt for the aerosol mass (Supplementary Fig. S8). In the Uniform case where the magnitude of global mean cooling is similar to the 1 × CO2 case (Supplementary Fig. S6), the global mean precipitation is reduced by 7.9% which is larger than the reduction in the 1 × CO2 case (−5.52%). These results are consistent with [34] and [36].

The spatial pattern of precipitation changes relative to 2 × CO2 is nearly similar in the Uniform, Tropic and Polar cases when compared to 1 × CO2 (Supplementary Fig. S8a). In the case of Arctic and Antarctic, however, there are major spatial pattern changes, and this can be attributed to the interhemispheric temperature difference leading to shift in the intertropical convergence zone (ITCZ; the latitudinal position of the ascending branch of the Hadley cells) [60, 63, 82]. The NH tropical region receives more rainfall in the Antarctic case with reduction in rainfall in the SH tropical region while the reverse is simulated in the Arctic case.

Several recent modeling studies have shown that the latitudinal position of ITCZ changes in response to changes in interhemispheric temperature differences [32, 47, 60, 63, 83–85]. For instance, an uneven radiative forcing due to the asymmetric distribution of dust aerosols shifts ITCZ position leading to changes in the tropical precipitation [86]. The change in the latitudinal location of ITCZ or equivalently tropical precipitation maximum can be quantified using precipitation centroid (Pcentroid) and

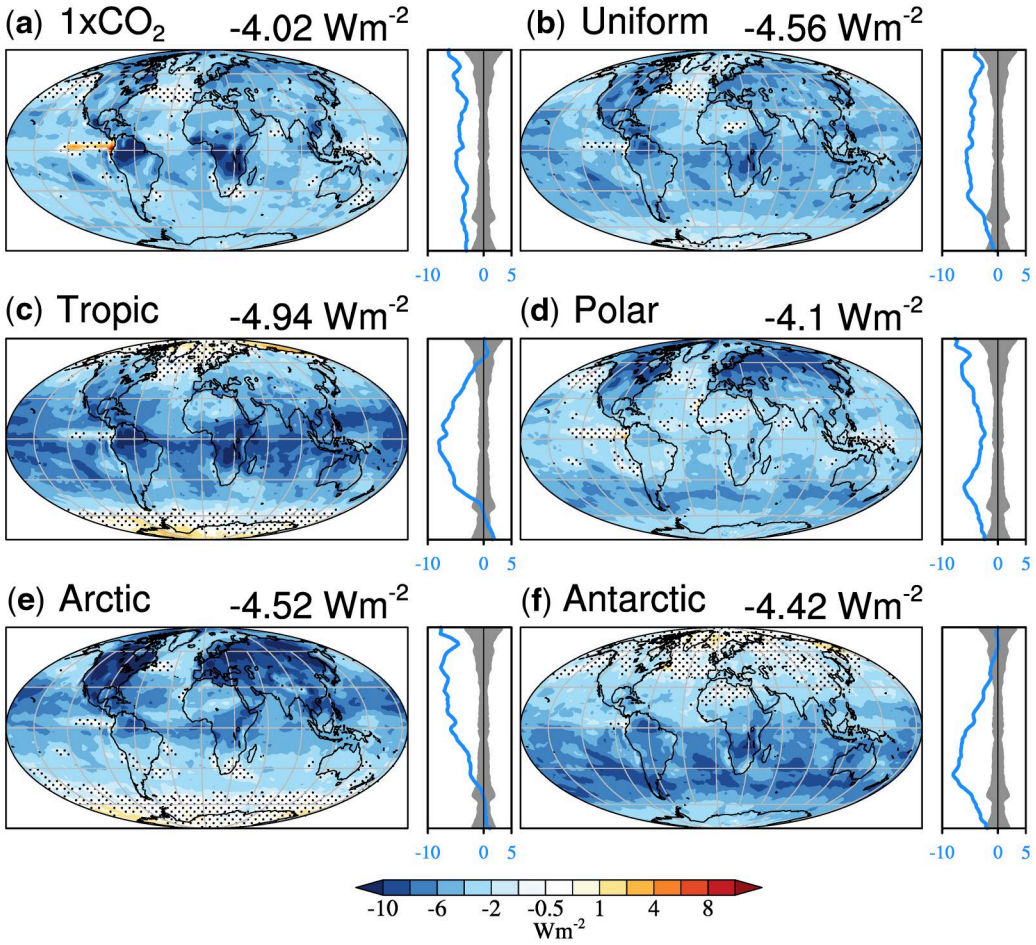

Figure 2. The spatial pattern of effective radiative forcing (ERF) for the 1 × CO2 and the five SAG simulations: (a) 1 × CO2, (b) Uniform, (c) Tropic, (d) Polar, (e) Arctic and (f) Antarctic, relative to 2 × CO2 with 25.76 Mt of volcanic sulfate aerosols prescribed in the stratosphere (23 hPa (~25 km) and 37 hPa (~22 km)). The change in global mean value is shown on the top right of each panel. Stippled areas show areas which are not significant at 95% confidence level estimated by student's *t*-test using the last 30 years of the 60 years prescribed-SST simulation. The side subpanel shows the zonal mean changes, and the shaded region (gray) represents ± 1 SD from the 1 × CO2 simulation.

Table 2. Changes in global mean and interhemispheric difference in AOD, ERF and TS in the 1 × CO2 and the five SAG simulations with 25.76 Mt of volcanic sulfate aerosols relative to the 2 × CO2 simulation

Variables	Experiment					
	1 × CO2	Uniform	Tropic	Polar	Arctic	Antarctic
ΔGMAOD	0	0.19	0.19	0.19	0.19	0.19
ΔGMERF (Wm^{-2})	−4.02 ± 0.05	−4.56 ± 0.05	−4.94 ± 0.06	−4.1 ± 0.05	−4.52 ± 0.05	−4.42 ± 0.05
ΔGMTS (K)	−3.22 ± 0.01	−3.23 ± 0.02	−2.88 ± 0.02	−3.58 ± 0.02	−2.96 ± 0.01	−3.52 ± 0.02
ΔIHAODD	0	0	0	0	0.18	−0.18
ΔIHERFD (Wm^{-2})	−0.17 ± 0.08	0.03 ± 0.07	0.14 ± 0.09	−0.05 ± 0.09	−3.71 ± 0.08	3.68 ± 0.08
ΔIHTSD (K)	−0.06 ± 0.02	0.07 ± 0.03	−0.14 ± 0.03	0.26 ± 0.03	−2.14 ± 0.03	2.21 ± 0.03

The interhemispheric differences are calculated as the difference between northern and southern hemispheric mean values.

this metric is defined as the median latitude of zonal mean area-weighted precipitation between 20° S and 20° N [87]. The mean latitudinal position of ITCZ is sensitive to the hemispherical asymmetry in forcing [85, 88, 89]. We calculate Pcentroid after interpolation of the precipitation data onto a 0.01° grid [47, 60, 87, 90, 91]. Cheng *et al.* [89] and Roose *et al.* [60] discussed the ITCZ shift with respect to inter-hemispheric surface temperature and AOD respectively. However, they do not discuss the response in ITCZ and precipitation to GMAOD. Therefore, in this study we study the ITCZ position change both in terms of both global mean and interhemispheric differences in AOD for a complete characterization. We find a sensitivity of about 0.36° ± 0.18° in the latitudinal position of ITCZ to GMAOD and −1.8° ± 0.04° to 0.1 IHAODD (Fig. 3). The slight northward shift in ITCZ for GMAOD is likely due to the difference in land-sea distribution between the two hemispheres. Though we have considered a larger number of SAG simulations here, the sensitivity of ITCZ position to IHAODD is similar to [60].

Precipitation indices

Global mean precipitation response

In this section, we examine the influence of AOD, ERF and TS on the global mean precipitation. About 4.37% decline in global

mean precipitation is simulated for every 0.1 increase in GMAOD (Fig. 4a) whereas a slight increase of 0.36% per 0.1 increase in IHAODD (Fig. 5a). The small sensitivity to IHAODD is likely due to the difference in land-sea distribution between the two hemispheres. The sensitivity of ERF and TS is also estimated (Fig. 6a). For each unit increase (Wm^{-2}) in GMERF and unit increase (K) in GMTS, global mean precipitation is seen to increase by 1.84% and 2.54% respectively. In the case of interhemispheric differences, global mean precipitation slightly decreases by 0.22% and 0.1% for per unit increase in IHERFD and IHTSD.

Thus, the global mean precipitation is mainly influenced by global mean AOD, ERF and TS and interhemispheric difference in these quantities have little influence. For asymmetric forcing with large interhemispheric differences, the precipitation increases in the warmer hemisphere with a compensating decrease in the other hemisphere (shift in ITCZ shown in Fig. 3b). The net result is only a slight change in the global mean precipitation and little sensitivity to the interhemispheric differences.

Northern hemisphere monsoon precipitation response

The NHMI has contribution from precipitation in the three NH monsoon regions: North African, North American and South Asian monsoon region. Figs 4b and 5b shows the changes in the northern hemisphere precipitation (%), for different amounts (25.76 Mt, 17.17 Mt and 8.08 Mt) of volcanic sulfate aerosols. We estimate a sensitivity of −1.33 ± 0.95% per 0.1 increase in GMAOD and −7.62 ± 0.03% per 0.1 increase in IHAODD. Thus, NHMI is more sensitive to IHAODD than to GMAOD.

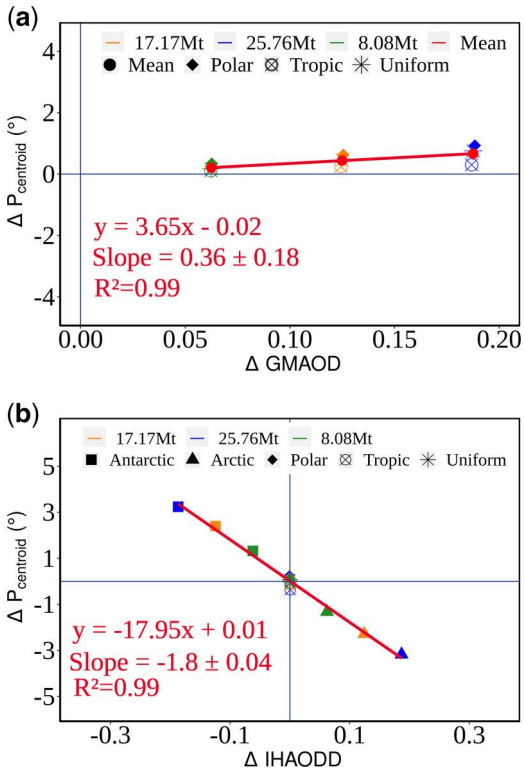

Figure 3. (a) Changes in precipitation centroid (Pcentroid) as a function of changes in GMAOD (global mean AOD). The red dots indicate the mean of the Uniform, Polar and Tropic cases with different aerosols amounts (25.76, 17.17 and 8.08 Mt). (b) Changes in precipitation centroid (Pcentroid) as a function of changes in IHAODD (interhemispheric AOD difference) in the Arctic and Antarctic cases with different aerosols amounts. The red line shows the best linear fit. The linear equation and slope (% per 0.1 GMAOD or IHAODD) are shown at bottom left of each panel. The uncertainty in slope is measured as one-half of the difference between the maximum and minimum slopes of the regression line [92].

The sensitivity of NHMI to global mean and interhemispheric difference in ERF and TS are also estimated (Supplementary Fig. S9) and the results are summarized in Fig. 6b. NHMI shows a sensitivity of 0.6 ± 0.4% per unit increase (Wm^{-2}) in GMERF and 0.8 ± 0.9% per unit increase (K) in GMTS. In case of interhemispheric differences, 3.79 ± 0.08% and 6.46 ± 0.06% per unit increase (Wm^{-2} and K) in IHERFD and IHTSD respectively is estimated. Similar to AOD, NHMI shows larger sensitivity to interhemispheric differences in ERF and TS than to respective global means.

The precipitation response shows some degree of nonlinearity with respect to GMAOD. As shown in Table 2, the reduction in global mean surface temperature is most pronounced for the Polar case and least for the Tropic case though the GMAOD changes are the same. This spread in surface temperature response for same GMAOD arises because the global mean surface temperature change is larger when forcing is imposed in the polar regions [93, 94]. Given that surface temperature change is a primary driver of precipitation changes, the NHMI reduction is relatively larger for the polar case. However, we use a linear fit to provide a simpler assessment but the departure from linearity indicates the dependence of climate sensitivity on the latitudinal distribution of forcing even when the mean forcing is the same in the two hemispheres.

Southern hemisphere monsoon precipitation response

SHMI is the sum of summer monsoon precipitation from the South African, South American and Australian monsoon regions. We estimate a sensitivity of −5.08 ± 0.01% per 0.1 increase in GMAOD (Fig. 4c) and 3.91 ± 0.36% per 0.1 increase in IHAODD (Fig. 5c). SHMI has larger sensitivity to GMAOD which is likely related to a sensitivity of ∼0.4° northward shift in ITCZ to 0.1 increase in GMAOD (Fig. 3a). This leads to a larger sensitivity of SHMI to GMAOD than in case of NHMI (Fig. 4b and c, Supplementary Fig. S15b and d). Because of the differences in land-sea distribution between the hemispheres, we find that a symmetric forcing of aerosols results in a larger decrease in precipitation over SH. This is consistent with [95, 96].

SHMI is found to have similar sensitivity to global mean changes in ERF and TS and to respective changes in interhemispheric differences (Supplementary Fig. S10, Fig. 6c). For a unit increase in global mean ERF ($1\,Wm^{-2}$) and TS (1 K), SHMI increases by 2.1% and 3%, respectively. For similar increase in the interhemispheric differences, the respective changes (decreases) are 1.99% and 2.89%.

Tropical monsoon precipitation response

The tropical monsoon index (TMI) is the sum of NHMI and SHMI. For 0.1 increase in GMAOD, TMI decreases by 3.63 ± 0.1% (Fig. 4d), and for a similar increase in IHAODD, TMI changes by −0.54 ± 0.29% (Fig. 5d). For an increase in IHAODD, changes in NHMI and SHMI nearly cancel each other, hence the decrease in precipitation is mostly due to the increase in GMAOD as indicated by the y-intercept (∼ 0.28%; Fig. 5d).

Similar to AOD, the sensitivity of TMI (Supplementary Fig. S11, Fig. 6d) to global mean of ERF and TS is larger than the respective interhemispheric differences. TMI is found to increase by 1.5% and 2.1% for global mean ERF and TS increases of $1\,Wm^{-2}$ and 1 K, respectively. However, for similar increases in interhemispheric differences, the respective increases are only 0.24% and 0.71%.

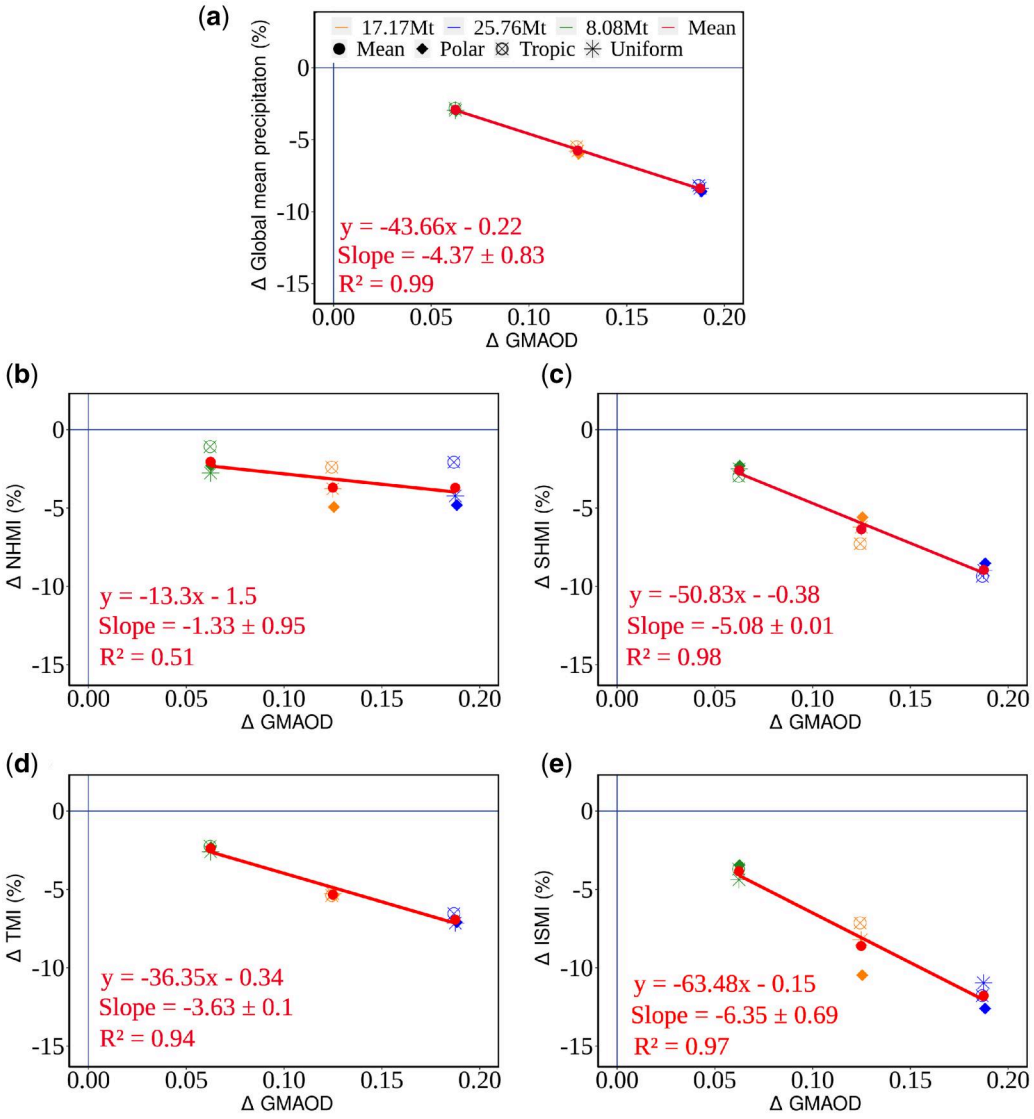

Figure 4. Changes in (a) global mean precipitation, (b) NHMI (northern hemisphere monsoon index), (c) SHMI (southern hemisphere monsoon index), (d) TMI (tropical monsoon index), and (e) ISMI (Indian summer monsoon index) as a function of GMAOD (Global mean AOD). The redline is the best linear fit. The regression equation with slope (% per 0.1 GMAOD) is shown on the bottom left of each panel. The uncertainty in slope is measured as one-half of the difference between the maximum and minimum slopes of the regression line [92].

Indian summer monsoon precipitation response

The Indian summer monsoon rainfall (June–September) contributes about 80% to India's annual mean rainfall [97, 98]. For our analysis over the Indian subcontinent, we have considered the June-September (JJAS) season, and the precipitation over India during this season is defined as the Indian summer monsoon index (ISMI). ISMI is found to reduce by 6.35 ± 0.69% per 0.1 increase in GMAOD and about 9.32 ± 0.47% per 0.1 increase in IHAODD (Figs 4e and 5e). The maximum reduction is seen in the case of the Arctic (25.76 Mt) with rainfall decrease of about −29.59% (Supplementary Fig. S13e). This is due to the southward shift in the ITCZ location in for the Arctic case as discussed in section "Precipitation response and ITCZ shift" (Fig. 3b). This southward shift is seen in most longitudes, and we demonstrate it for the Arctic and Antarctic simulations with 25.76 Mt of volcanic sulfate aerosols (Supplementary Fig. S14).

To illustrate the spatial distribution of the sensitivity of precipitation to GMAOD and IHAODD, we normalized the Indian summer monsoon precipitation changes by GMAOD and IHAODD (Fig. 7a and b). For an increase of 0.1 in GMAOD, precipitation decreases throughout the Indian subcontinent with a slight positive anomaly over the north and south. For every 0.1 increase in IHAODD, precipitation is suppressed over entire India except in the northeast where there is slight increase in precipitation. The spatial pattern of ISMI sensitivity to GMAOD follows the ISMI response to the Uniform, Tropic and Polar cases (symmetric aerosol distribution) (Supplementary Fig. S13b–d) while the sensitivity to IHAODD follows the ISMI response in the Arctic and Antarctic cases (asymmetric aerosol distribution) (Supplementary Fig. S13e and f). The domain mean value of ISMI per 0.1 increase in GMAOD and IHAODD (Fig. 7) are in good agreement with the mean sensitivity calculated in Figs 4e and 5e. The sensitivity of ISMI to the global mean and interhemispheric difference in ERF and TS is found to be positive with larger sensitivity to interhemispheric differences (Supplementary Fig. S12, Fig. 6e).

Regional monsoon precipitation responses

The North American monsoon region shows an increase in precipitation in all simulations (Fig. 8a) with a maximum magnitude

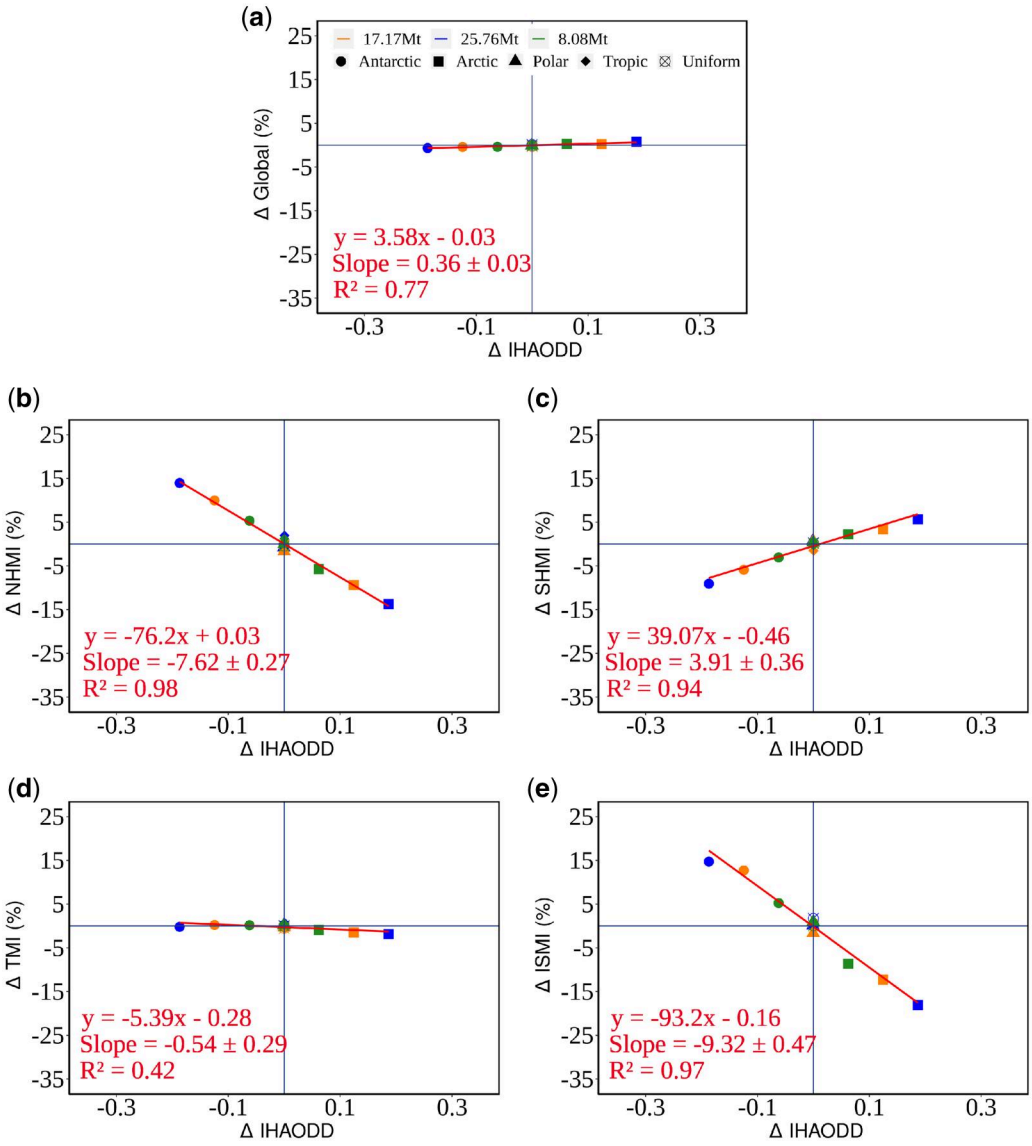

Figure 5. Changes (%) in (a) global mean precipitation, (b) NHMI (northern hemisphere monsoon index), (c) SHMI (southern hemisphere monsoon index), (d) TMI (tropical monsoon index), and (e) ISMI (Indian summer monsoon index) as a function of IHAODD (Interhemispheric AOD difference). The redline is the best linear fit. The regression equation with slope (% per 0.1 IHAODD) is shown on the bottom left of each panel. The uncertainty in slope is measured as one-half of the difference between the maximum and minimum slopes of the regression line [92].

in the case of Antarctic simulation where the ITCZ shifts northward by 3.9° for 25.76 Mt of volcanic sulfate aerosols (Fig. 3b). The increase is the least in the Arctic case where the ITCZ shifts southward by about 2.5° (Fig. 3b). In the case of North African monsoon domain, increase in precipitation is simulated in the Antarctic and Tropic cases (Fig. 8b) and this is also evident in the spatial pattern of precipitation changes (Supplementary Fig. S8). An overall reduction in precipitation for all the cases is simulated for the other regions, indicating a dominant influence of the increase in GMAOD.

In the case of Arctic simulation, more aerosol is prescribed in the northern hemisphere. This causes a larger cooling in the northern hemisphere and the precipitation centroid (ITCZ) shifts south of its normal position by 3.18°, 2.29° and 1.33° latitude for 25.76, 17.17 and 8.08 Mt of aerosol loading simulations respectively (Fig. 3b). This asymmetric cooling causes a reduction in regional rainfall in the northern hemisphere ([99], Supplementary Fig. S15a and c) with the largest decrease for the case with 25.76 Mt prescribed volcanic aerosols. Conversely, when there is a larger aerosol loading in the southern hemisphere, the increased cooling in that hemisphere causes a shift of the ITCZ northward by about 3.2°, 2.4° and 1.3° in latitude for the three aerosols amounts (Fig. 3b). This northward ITCZ shift results in increased precipitation in the northern hemisphere monsoon regions (Fig. 8, Supplementary Fig. S15a and c).

It is also found that the southern hemisphere monsoon regions show least reduction for the Arctic case irrespective of the aerosol amount. Broadly, our results are consistent with recent studies which show that when sulfate aerosols are injected in high latitudes in the northern hemisphere there is precipitation reduction over north Africa and south Asian monsoon regions and when aerosols are is injected in the southern hemisphere high latitude, north African monsoon precipitation increases [32, 59, 88]. It may be noted that we have not calculated

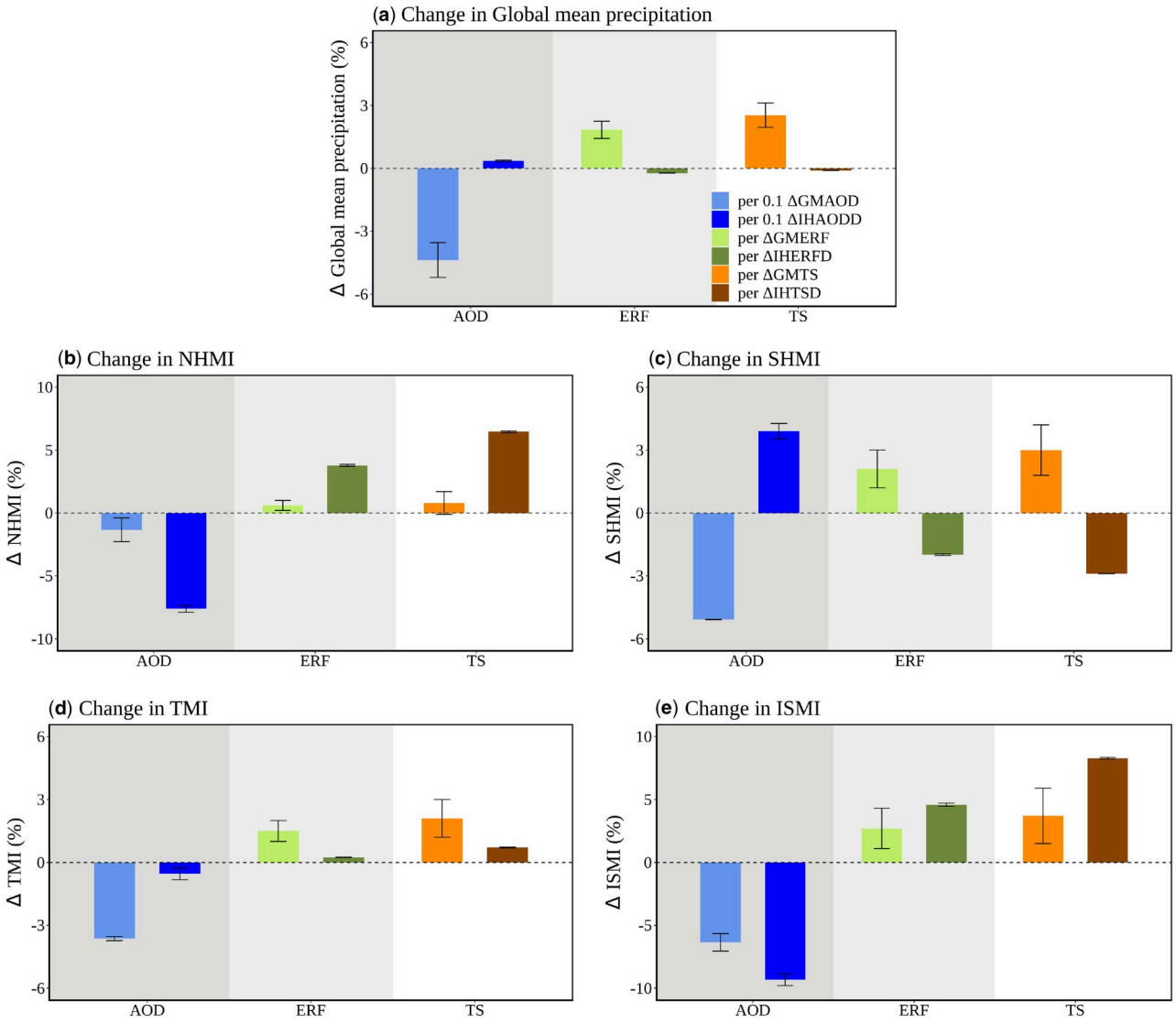

Figure 6. Sensitivity (%) of (a) global mean precipitation, (b) NHMI (northern hemisphere monsoon index), (c) SHMI (southern hemisphere monsoon index), (d) TMI (tropical monsoon index) and (e) ISMI (Indian summer monsoon index) to per unit (0.1 for AOD, 1 Wm^{-2} for ERF, and 1 K for TS) changes in global mean and interhemispheric difference in AOD (aerosol optical depth), ERF (effective radiative forcing) and TS (surface temperature). Error bars represent uncertainty, measured as one-half of the difference between the maximum and minimum slopes of the regression line [92].

the sensitivity parameters for each regional monsoon domain, but the same methodology used for NHMI, SHMI, TMI and ISMI can be applied in principle.

Validation

In order to validate our framework (Equation 1), we have performed additional simulations as discussed in section "Validation experiments." The latitudinal distribution of aerosols in these simulations are selected such that these distributions differed fundamentally from those used to estimate the sensitivity parameters. We estimate the changes in precipitation for all the precipitation indices considered in our study using Equation (1) and compare them with the model simulated precipitation changes (Supplementary Table S2). These changes are all computed relative to the control run (2 × CO2). For the validation, the root mean square error (RMSE) between the estimated and model simulated precipitation changes are calculated (Fig. 9).

For the global mean precipitation, the RMSE is found to be 0.29%, while for the tropical monsoon indices TMI, NHMI and SHMI, RMSE is 0.88%, 1.91% and 2% respectively (Fig. 9). However, in the case of the Indian summer monsoon precipitation index (ISMI), the RMSE value is slightly larger at 2.83%. Clustering of the points near the dashed line in Fig. 9 indicates that estimated precipitation changes are in good agreement with the model precipitation changes. The RMSE is calculated between the spatio-temporally averaged model simulated and estimated precipitation from our framework (Equation 1).

Thus, in the validation simulations, the estimated precipitation changes are close to the model simulated precipitation changes. The estimated and model simulated precipitation are also in good agreement when the formulation is framed, in terms of effective radiative forcing and surface temperature (Equations (2) and (3); Supplementary Figs S16 and S17; Supplementary Tables S3 and S4). We also performed the validation for the 15 experiments with which the sensitivity was estimated

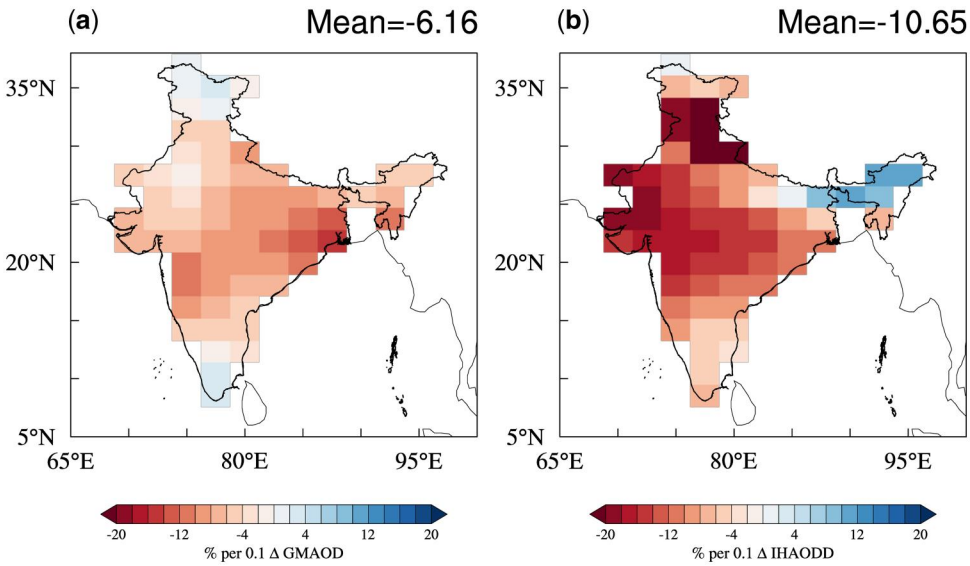

Figure 7. The spatial pattern of changes in ISMI (Indian summer monsoon index; %) per 0.1 increase in (a) GMAOD (global mean AOD) and (b) IHAODD (interhemispheric AOD difference). The domain mean (%) is shown in the top right of the panels.

(Supplementary Table S5). The estimated sensitivity coefficients (Equations 1–3) are listed in Supplementary Table S6 and the changes in the global mean and interhemispheric difference in AOD, ERF and TS for the validation experiments are shown in Supplementary Table S7.

Discussions and summary

In this paper, as an extension to [60], we performed additional SAG simulations with varying amounts of volcanic aerosols to estimate the sensitivity of the tropical monsoon precipitation to unit changes in global mean and interhemispheric differences in AOD, ERF and surface temperature. We have proposed that the tropical monsoon precipitation changes under SAG are mainly influenced by two mechanisms: (i) The cooling effects of sulfate stratospheric aerosols due to an increase in GMAOD lead to a reduction in precipitation. (ii) A change in IHAODD causes a shift in ITCZ toward the warmer hemisphere, thereby changing the precipitation patterns in the tropics. Hence, we propose that the changes in the tropical monsoon precipitation due to aerosols in the stratosphere can be determined by two key AOD parameters (Equation 1): the global mean AOD, and the interhemispheric AOD difference.

We use simulations with a symmetric aerosol distribution i.e. Uniform, Tropic and Polar for estimating the sensitivity to GMAOD. Next, we remove the influences of GMAOD from the precipitation indices to obtain the IHAODD influence for all the regressions with respect to IHAODD. Hence, we estimate the sensitivity of the tropical monsoon precipitation to IHAODD using all the 15 simulations. The reduction in monsoon precipitation indices, NHMI, SHMI, TMI and ISMI with an increase in GMAOD is evident in Fig. 4.

Our formulation based on planetary energetics represented by Equation (1) is validated by performing an additional set of simulations with different meridional distribution of aerosols. The precipitation estimated using Equation (1) is in good agreement with the model simulated precipitation. This verifies our hypothesis that the change in the global mean precipitation and the tropical monsoon indices can be estimated to a very good accuracy using just two independent parameters: the global mean AOD and the interhemispheric AOD difference. We find good agreement as the residuals are too small, indicating that the two factors, GMAOD and IHAODD can explain most of the changes in the tropical monsoon precipitation. We have also demonstrated that the formulation could be framed, instead of AOD, in terms of effective radiative forcing and surface temperature as well (Equations 2 and 3; Supplementary Figs S16 and S17; Supplementary Tables S3 and S4). Supplementary Table S8 shows the quotient (ratio) between the responses to global mean and interhemispheric differences in AOD, ERF and TS, which clearly shows that our approach is effective for NHMI, SHMI, and ISMI. However, the influence of interhemispheric differences on global mean precipitation and TMI sensitivity are too small, and hence we find large variations in the ratios. Nonetheless, it is intriguing to note that the order of magnitudes of these ratios are the same for the global mean precipitation and TMI, indicating a near-linear behavior in these cases too.

However, there are several limitations to our study. First, we have considered idealized distributions of aerosols which may be challenging to achieve in the real world. Second, our slab-ocean simulations do not include the effects of deep ocean dynamics and transient climate response. A coupled model simulation would enable the assessment of transient climate response. As ocean heat transport is fixed in slab ocean simulations, the required heat transport changes are reflected in atmospheric transport only. Hence, the ITCZ shift and the corresponding monsoon precipitation response are likely overestimated in the slab ocean simulations [60]. Third, we prescribe aerosols, and their concentrations do not vary with season. Thus, our simulations do not include the effects of complex processes like aerosol transport, microphysics, chemistry, and sedimentation. Recent studies [33, 100–102] have shown that the season of injection, transport and aerosol physics and chemistry have strong influence on the spatial distribution of injected aerosols.

Fourth, we focused mainly on two parameters to explain the tropical monsoon precipitation changes. However, it is important to note that regional monsoon precipitation is also influenced by various other factors such as regional geometry and geography.

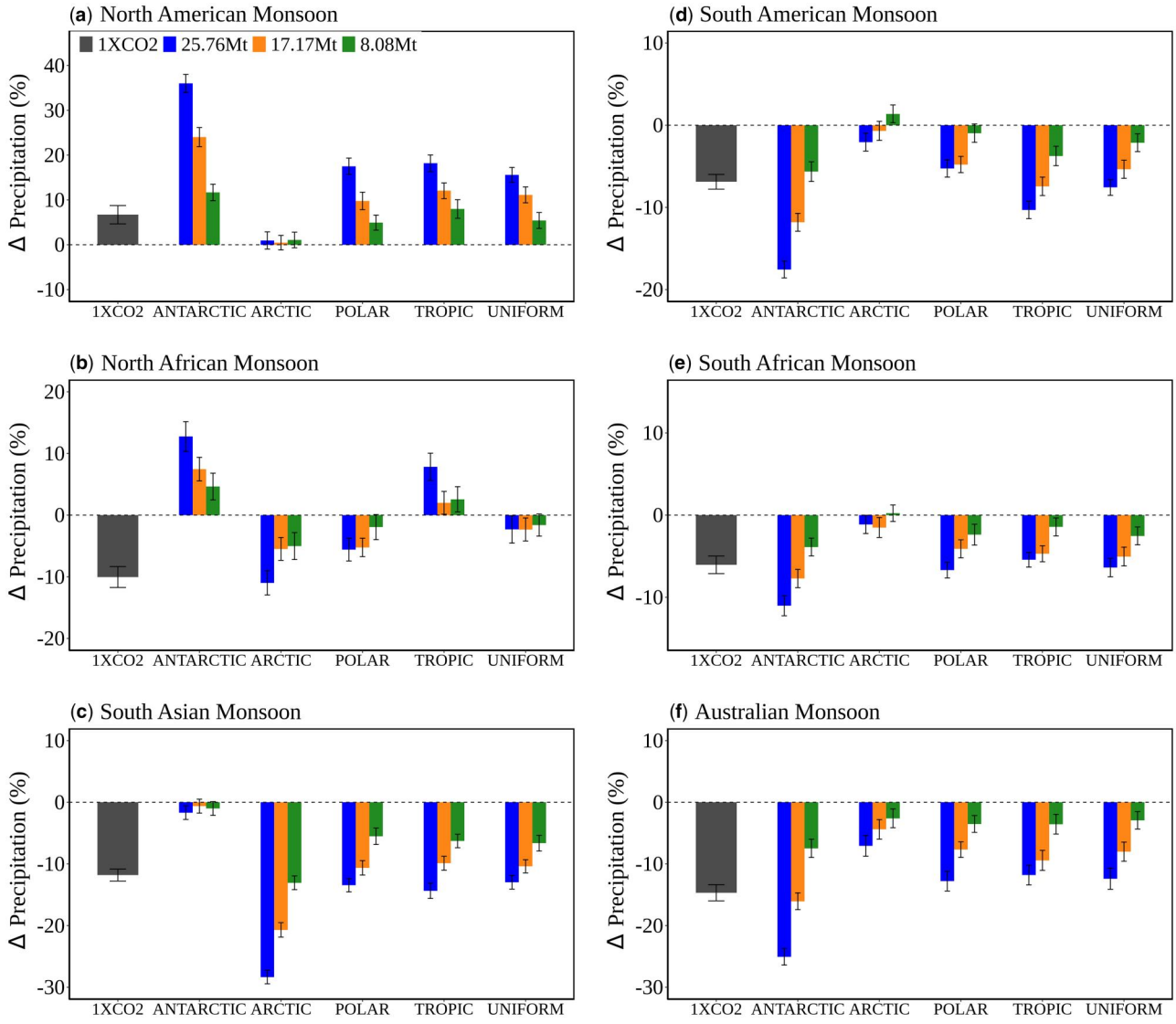

Figure 8. Changes (%) in summer monsoon precipitation in the 1 × CO2 simulation and in the five SAG experiments for three amounts of prescribed aerosols (25.76, 17.17, 8.08 Mt) relative to the 2 × CO2 simulation for the northern hemisphere monsoon regions (a–c) and the southern hemisphere monsoon regions (d–f). The error bars show the standard error derived from the last 60 years of the 100-year slab-ocean simulations.

Other planetary scale factors such as equator to pole gradient in AOD may also have influence. These additional factors might account for the disparities between our estimated and model simulated precipitation changes. Fifth, we have only investigated the radiative effects of stratospheric aerosols and hence the effects of aerosol-cloud interaction that is important for the tropospheric aerosols are not represented in our simulations; future research should examine the potential of extending this framework to understand the link between tropospheric aerosols and the tropical monsoon precipitation. Sixth, it should be noted that only reflective aerosols are considered in this study. In the case of absorbing type of aerosols, the effect could be opposite to the results presented here [103, 104]. Seventh, we have not studied the sensitivity to the altitude or size of the aerosol particles. An investigation of the sensitivity to altitude and particle size of aerosols merits further studies. Eight, we have studied only the mean monsoon precipitation changes and did not investigate variability. We do recognize the importance of monsoon variability on interannual and decadal timescales to agriculture and water resources. Investigation of changes in variability for SAG merits further studies.

Ninth, the proposed formulation is only used for the tropical monsoon precipitation changes in our study, and its validity for the extra-tropical precipitation is yet to be explored. We have not attempted to explain the differences in sensitivity factors, for example between NHMI and SHMI. We recognize that the regional monsoon responses would differ as regional geometry could play an important role in determining the sensitivity factors for individual monsoon regions. It is important to note that we have presented a simpler framework based on planetary energetics in this paper to explain large scale changes in precipitation in the tropics. We intend to identify the causes for the differences in sensitivity factors for individual regional monsoon regions and also between NHMI and SHMI in future studies. Tenth, we recognize that CAM4 is an older version and newer versions simulate the climate better. Our investigation is a sequel to an earlier study from our group [60], which used CAM4. CAM4 is computationally inexpensive compared to later versions, CAM5 and

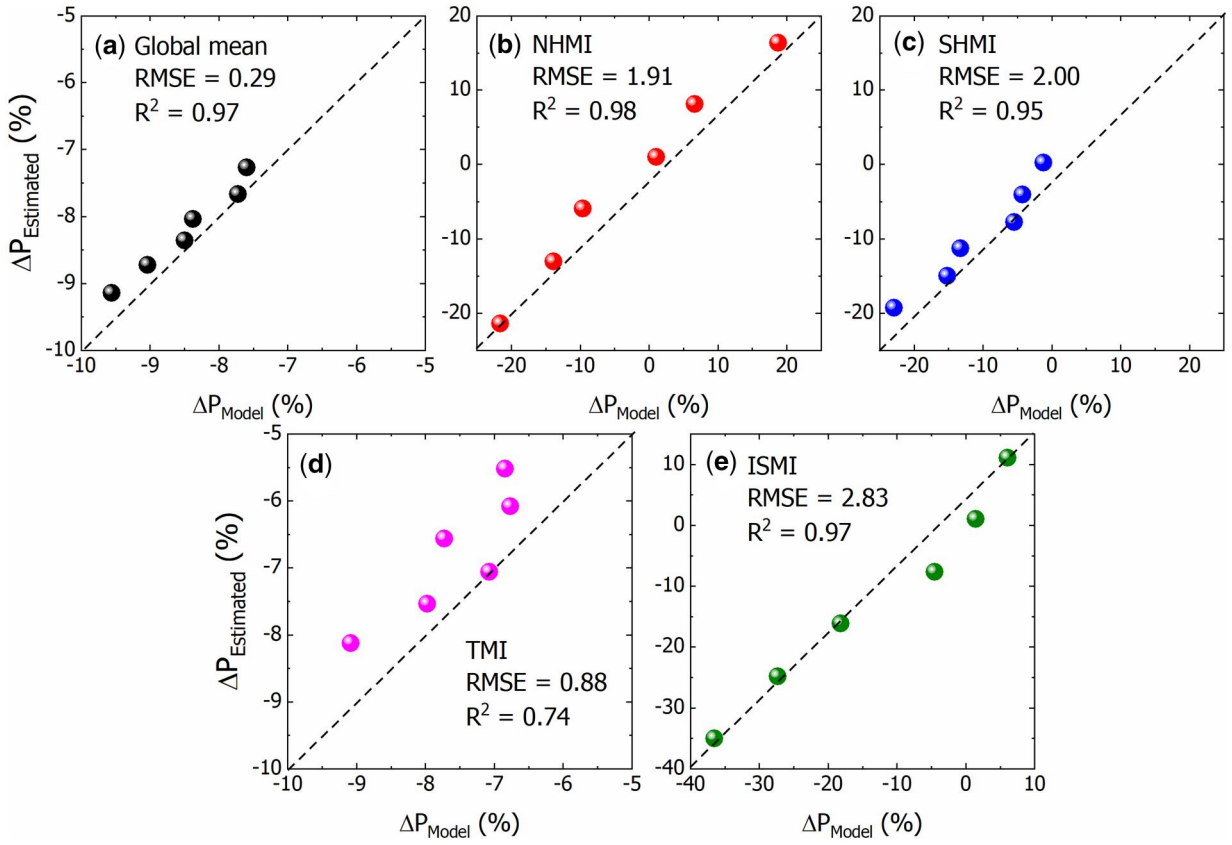

Figure 9. Scatter plot between estimated precipitation change (%; Equation 1) and model simulated precipitation for the (a) global mean, (b) NHMI (northern hemisphere monsoon index), (c) SHMI (southern hemisphere monsoon index), (d) TMI (tropical monsoon index), and (e) ISMI (Indian summer monsoon index) with their RMSE (%) values. Dashed lines show 1 : 1 curve (identity line). The subplots have different x-axis and y-axis scales.

CAM6. Therefore, to ensure consistency, continuation and cheaper computational costs we have used CAM4. However, we believe that the qualitative findings of our study will remain unchanged in simulations using later versions. Finally, our study uses simulations from a single climate model. Further studies using multiple comprehensive coupled climate models are needed in the future to assess the robustness of the results presented here.

Despite these limitations, we believe our findings are fundamental as we have relied on basic constraints in planetary energetics to explain the tropical monsoon precipitation change. The framework proposed here (Equation 1) provides valuable guidance to understand the tropical precipitation changes in terms of a single variable (AOD) in case of a potential SAG deployment. The framework could be also useful in estimating the tropical monsoon precipitation changes for past and future volcanic eruptions. Further, if extended to tropospheric aerosols with appropriate modifications to account for aerosol-cloud interactions, it could provide insight into historical changes in monsoon precipitation caused by tropospheric aerosols.

Acknowledgements

This work was funded by the Degrees Initiative [RGA- DMF23IND] and the Department of Science and Technology (DST), Government of India grants [DST/NSM/R&D_HPC_Applications/2021/03.09 and DST/CCP/NMSKCC/MRDP/210/2022(G)]. We would like to acknowledge the high-performance computing support from the Supercomputer Education and Research Centre (SERC) team, Indian Institute of Science, Bangalore. We are thankful to the CESM team for maintaining and managing the code.

Author contributions

Anu Xavier (Conceptualization [Equal], Data curation [Equal], Formal analysis [Equal], Investigation [Equal], Methodology [Equal], Software [Equal], Validation [Equal], Visualization [Equal], Writing—original draft [Equal], Writing—review & editing [Equal]), Govindasamy Bala (Conceptualization [Equal], Formal analysis [Equal], Funding acquisition [Equal], Methodology [Equal], Project administration [Equal], Supervision [Equal], Writing—original draft [Equal], Writing—review & editing [Equal]), Shinto Roose (Methodology [Equal], Writing—review & editing [Equal]), Usha K H (Writing—review & editing [Equal])

Supplementary data

Supplementary data is available at *Oxford Open Climate Change* online.

Conflict of interest: None declared.

Funding

Degrees Initiative [RGA- DMF23IND].

Data availability

The data underlying this article will be shared on reasonable request to the corresponding author.

References

1. Gulev SK, Thorne PW, Ahn J *et al.* Changing state of the climate system. In: *Climate Change 2021—The Physical Science Basis*. UK: Cambridge University Press,2021, 287–422.
2. IPCC. *Climate Change 2022 - Mitigation of Climate Change Contribution of Working Group III to the Sixth Assessment Report of the Intergovernmental Panel on Climate Change [P.R. Shukla, J. Skea, R. Slade, A. Al Khourdajie, R. van Diemen, D. McCollum, M. Pathak, S. Some, P. Vyas, R. Fradera, M. Belkacemi, A. Hasija, G. Lisboa, S. Luz, J. Malley, (Eds.)*. UK: Cambridge University Press, 2022.
3. Calvin K, Dasgupta D, Krinner G *et al. IPCC, 2023: Climate Change 2023: Synthesis Report. Contribution of Working Groups I, II and III to the Sixth Assessment Report of the Intergovernmental Panel on Climate Change [Core Writing Team, H. Lee and J. Romero (Eds.)]*. Geneva, Switzerland: IPCC, 2023.
4. Matthews HD, Wynes S. Current global efforts are insufficient to limit warming to 1.5°C. *Science* 2022;**376**:1404–9.
5. Robock A. Stratospheric aerosol geoengineering. *AIP Conf Proc* 2015;**1652**:183–97.
6. Sognnaes I, Gambhir A, van de Ven DJ *et al.* A multi-model analysis of long-term emissions and warming implications of current mitigation efforts. *Nat Clim Chang* 2021;**11**:1055–62.
7. van de Ven DJ, Mittal S, Gambhir A *et al.* A multimodel analysis of post-Glasgow climate targets and feasibility challenges. *Nat Clim Chang* 2023;**13**:570–8.
8. Visioni D, Bednarz EM, MacMartin DG *et al.* The choice of baseline period influences the assessments of the outcomes of stratospheric aerosol injection. *Earths Future* 2023;**11**(8):e2023EF003851. https://doi.org/10.1029/2023EF003851.
9. Allen MR, Dube, OP, Solecki, W *et al.* Framing and context. In: *Global Warming of 1.5°C*. UK: Cambridge University Press, 2018, 49–92.
10. Caldeira K, Bala G, Cao L. The science of geoengineering. *Annu Rev Earth Planet Sci* 2013;**41**:231–56.
11. Crutzen PJ. Albedo enhancement by stratospheric sulfur injections: a contribution to resolve a policy dilemma? *Clim Change* 2006;**77**:211–20.
12. Kravitz B, Robock A, Boucher O *et al.* The geoengineering model intercomparison project (GeoMIP). *Atmospheric Science Letters* 2011;**12**:162–7.
13. Muthyala R, Bala G, Nalam A. Regional scale analysis of climate extremes in an SRM geoengineering simulation, part 1: precipitation extremes. *Curr Sci* 2018;**114**:1024.
14. Keith DW. Geoengineering the climate: history and prospect. *Annu Rev Energy Environ* 2000;**25**:245–84.
15. Modak A, Bala G. Sensitivity of simulated climate to latitudinal distribution of solar insolation reduction in solar radiation management. *Atmos Chem Phys* 2014;**14**:7769–79.
16. Shepherd JG. *Geoengineering the Climate: Science, Governance and Uncertainty*. London, GB: Royal Society, 2009.
17. Bala G, Gupta A. Solar geoengineering research in India. *Bull Am Meteorol Soc* 2019;**100**:23–8.
18. Bickel JE, Agrawal S. Reexamining the economics of aerosol geoengineering. *Clim Change* 2013;**119**:993–1006.
19. Keith DW. Photophoretic levitation of engineered aerosols for geoengineering. *Proc Natl Acad Sci U S A* 2010;**107**:16428–31.
20. Smith W. The cost of stratospheric aerosol injection through 2100. *Environ Res Lett* 2020;**15**:114004.https://doi.org/10.1088/1748-9326/aba7e7.
21. Cao L, Duan L, Bala G *et al.* Simultaneous stabilization of global temperature and precipitation through cocktail geoengineering. *Geophys Res Lett* 2017;**44**:7429–37.
22. Latham J. Control of global warming. *Nature* 1990;**347**:339–40.
23. National Academies of Sciences E and M. *Reflecting Sunlight: Recommendations for Solar Geoengineering Research and Research Governance*. Washington, DC: National Academies Press, 2021.
24. Niemeier U, Schmidt H, Alterskjær K *et al.* Solar irradiance reduction via climate engineering: Impact of different techniques on the energy balance and the hydrological cycle. *Jgr Atmospheres* 2013;**118**(21):11–905. https://doi.org/10.1002/2013JD020445.
25. United Nations Environment Programme. *One Atmosphere: An Independent Expert Review on Solar Radiation Modification Research and Deployment*. Kenya, Nairobi: UNEP, 2023.
26. Kleinschmitt C, Boucher O, Platt U. Sensitivity of the radiative forcing by stratospheric sulfur geoengineering to the amount and strategy of the SO_2 injection studied with the LMDZ-S3A model. *Atmos Chem Phys* 2018;**18**:2769–86.
27. Krishnamohan KS, Bala G, Cao L *et al.* Climate system response to stratospheric sulfate aerosols: Sensitivity to altitude of aerosol layer. *Earth Syst Dynam* 2019;**10**:885–900.
28. Krishnamohan KS, Bala G, Cao L *et al.* The climatic effects of hygroscopic growth of sulfate aerosols in the stratosphere. *Earths Future* 2020;**8**(2):e2019EF001326. https://doi.org/10.1029/2019EF001326.
29. Lee WR, Visioni D, Bednarz EM *et al.* Quantifying the efficiency of stratospheric aerosol geoengineering at different altitudes. *Geophys Res Lett* 2023;**50**(14):e2023GL104417. https://doi.org/10.1029/2023GL104417.
30. MacMartin DG, Kravitz B, Tilmes S *et al.* The climate response to stratospheric aerosol geoengineering can be tailored using multiple injection locations. *Jgr Atmospheres* 2017;**122**(23):12–574. https://doi.org/10.1002/2017JD026868.
31. Tilmes S, Richter JH, Mills MJ *et al.* Sensitivity of Aerosol Distribution and Climate Response to Stratospheric SO_2 Injection Locations. *Jgr Atmospheres* 2017;**122**(23):12–591. https://doi.org/10.1002/2017JD026888.
32. Krishnamohan KS, Bala G. Sensitivity of tropical monsoon precipitation to the latitude of stratospheric aerosol injections. *Clim Dyn* 2022;**59**:151–68.
33. Visioni D, MacMartin DG, Kravitz B *et al.* Seasonally modulated stratospheric aerosol geoengineering alters the climate outcomes. *Geophys Res Lett* 2020;**47**(12):e2020GL088337. https://doi.org/10.1029/2020GL088337.
34. Bala G, Duffy PB, Taylor KE. Impact of geoengineering schemes on the global hydrological cycle. *Proc Natl Acad Sci U S A* 2008;**105**:7664–9.
35. Kravitz B, MacMartin DG. Uncertainty and the basis for confidence in solar geoengineering research. *Nat Rev Earth Environ* 2020;**1**:64–75.
36. Tilmes S, Fasullo J, Lamarque J *et al.* The hydrological impact of geoengineering in the Geoengineering Model Intercomparison Project (GeoMIP). *Jgr Atmospheres* 2013;**118**(19):11–036. https://doi.org/10.1002/jgrd.50868.
37. Tilmes S, Mills M. Stratospheric sulfate aerosols and planetary albedo. In: *Global Environmental Change, Handbook of Global Environmental Pollution*. Netherlands: Springer, 2014, 771–6.

38. Heckendorn P, Weisenstein D, Fueglistaler S *et al.* The impact of geoengineering aerosols on stratospheric temperature and ozone. *Environ Res Lett* 2009;**4**:045108.
39. Pitari G, Aquila V, Kravitz B *et al.* Stratospheric ozone response to sulfate geoengineering: Results from the Geoengineering Model Intercomparison Project (GeoMIP). *Jgr Atmospheres* 2014;**119**:2629–53.
40. Tilmes S, Müller R, Salawitch R. The sensitivity of polar ozone depletion to proposed geoengineering schemes. *Science* 2008; **320**:1201–4.
41. Tilmes S, Visioni D, Jones A *et al.* Stratospheric ozone response to sulfate aerosol and solar dimming climate interventions based on the G6 Geoengineering Model Intercomparison Project (GeoMIP) simulations. *Atmos Chem Phys* 2022;**22**:4557–79.
42. Xia L, Nowack PJ, Tilmes S *et al.* Impacts of stratospheric sulfate geoengineering on tropospheric ozone. *Atmos Chem Phys* 2017;**17**:11913–28.
43. Irvine PJ, Kravitz B, Lawrence MG *et al.* Towards a comprehensive climate impacts assessment of solar geoengineering. *Earths Future* 2017;**5**:93–106.
44. Robock A. Benefits and risks of stratospheric solar radiation management (geoengineering). *Bridge (Kans City)* 2020; **50**:59–67.
45. Zarnetske PL, Gurevitch J, Franklin J *et al.* Potential ecological impacts of climate intervention by reflecting sunlight to cool Earth. *Proc Natl Acad Sci USA* 2021;**118**:
46. Lutsko NJ, Seeley JT, Keith DW. Estimating impacts and trade-offs in solar geoengineering scenarios with a moist energy balance model. *Geophys Res Lett* 2020;**47**(9): e2020GL087290. https://doi.org/10.1029/2020GL087290.
47. Nalam A, Bala G, Modak A. Effects of Arctic geoengineering on precipitation in the tropical monsoon regions. *Clim Dyn* 2018;**50**:3375–95.
48. Jones A, Haywood JM, Alterskjær K *et al.* The impact of abrupt suspension of solar radiation management (termination effect) in experiment G2 of the Geoengineering Model Intercomparison Project (GeoMIP). *Jgr Atmospheres* 2013; **118**:9743–52.
49. Kim DH, Shin HJ, Chung IU. Geoengineering: impact of marine cloud brightening control on the extreme temperature change over East Asia. *Atmosphere (Basel)* 2020;**11**:1345. https://doi.org/10.3390/atmos11121345.
50. Matthews HD, Caldeira K. Transient climate–carbon simulations of planetary geoengineering. *Proc Natl Acad Sci U S A* 2007;**104**:9949–54.
51. Hsu P, Li T, Wang B. Trends in global monsoon area and precipitation over the past 30 years. *Geophys Res Lett* 2011;**38** (8):L08701.
52. Wang B, Ding Q. Changes in global monsoon precipitation over the past 56 years. *Geophys Res Lett* 2006;**33**(6):L06711. https://doi.org/10.1029/2005GL025347.
53. Wang B, Ding Q. Global monsoon: Dominant mode of annual variation in the tropics. *Dynamics of Atmospheres and Oceans* 2008;**44**:165–83.
54. IPCC. Summary for Policymakers. In: Masson-Delmotte V, Zhai P, Pörtner H-O *et al.* (eds), *Global Warming of 1.5°C*. Cambridge, UK: Cambridge University Press, 2018, 3–24.
55. IPCC. *Climate Change 2014: Synthesis Report. Contribution of Working Groups I, II and III to the Fifth Assessment Report of the Intergovernmental Panel on Climate Change.[Core Writing Team, R. K. Pachauri and L.A. Meyer (Eds.)]*. Geneva, Switzerland: IPCC, 2014.
56. Govindasamy B, Caldeira K. Geoengineering Earth's radiation balance to mitigate CO_2-induced climate change. *Geophys Res Lett* 2000;**27**:2141–4.
57. Schmidt H, Alterskjær K, Karam DB *et al.* Solar irradiance reduction to counteract radiative forcing from a quadrupling of CO_2: climate responses simulated by four earth system models. *Earth Syst Dynam* 2012;**3**:63–78.
58. Bhowmick M, Mishra SK, Kravitz B *et al.* Response of the Indian summer monsoon to global warming, solar geoengineering and its termination. *Sci Rep* 2021;**11**:9791.https://doi.org/10.1038/s41598-021-89249-6.
59. Robock A, Oman L, Stenchikov GL. Regional climate responses to geoengineering with tropical and Arctic SO_2 injections. *J Geophys Res* 2008;**113**:D16101. https://doi.org/10.1029/2008JD010050.
60. Roose S, Bala G, Krishnamohan KS *et al.* Quantification of tropical monsoon precipitation changes in terms of interhemispheric differences in stratospheric sulfate aerosol optical depth. *Clim Dyn* 2023;**61**:4243–58.
61. Simpson IR, Tilmes S, Richter JH *et al.* The regional hydroclimate response to stratospheric sulfate geoengineering and the role of stratospheric heating. *Jgr Atmospheres* 2019; **124**:12587–616.
62. Broccoli AJ, Dahl KA, Stouffer RJ. Response of the ITCZ to northern hemisphere cooling. *Geophys Res Lett* 2006;**33**:1–4. https://doi.org/10.1029/2005GL024546.
63. Zhao M, Cao L, Bala G *et al.* Climate response to latitudinal and altitudinal distribution of stratospheric sulfate aerosols. *Jgr Atmospheres* 2021;**126**(24):e2021JD035379. https://doi.org/10.1029/2021JD035379.
64. Gent PR, Danabasoglu G, Donner LJ *et al.* The community climate system model version 4. *J Climate* 2011;**24**:4973–91.
65. Neale RB, Richter JH, Conley AJ *et al. Description of the NCAR Community Atmosphere Model (CAM 4.0)*. NCAR Tech. Note Ncar/TN-485+ STR. National Center for Atmospheric Research, Boulder, Colorado, USA, 2010.
66. Neale RB, Richter J, Park S *et al.* The mean climate of the community atmosphere model (CAM4) in forced SST and fully coupled experiments. *J Clim* 2013;**26**:5150–68.
67. Oleson K, DML, Bonan GB *et al.* Technical description of version 4.0 of the community land model (CLM). *NCAR Tech Note NCAR/TN-478+ STR* 2010;**257**:1–257.
68. Bailey D, Holland M, Hunke E *et al. Community ice CodE (CICE) user's guide version* 4.0. Boulder, Colorado: National Center for Atmospheric Research, 2010, p. 22.
69. Ban-Weiss GA, Caldeira K. Geoengineering as an optimization problem. *Environ Res Lett* 2010;**5**:034009.https://doi.org/10.1088/1748-9326/5/3/034009.
70. Neely Iii RR, Conley AJ, Vitt F *et al.* consistent prescription of stratospheric aerosol for both radiation and chemistry in the Community Earth System Model (CESM1). *Geosci Model Dev* 2016;**9**:2459–70.
71. Hansen J, Sato M, Ruedy R. Radiative forcing and climate response. *J Geophys Res* 1997;**102**:6831–64.
72. Myhre GD, Shindell F-M, Bréon WC *et al.* Anthropogenic and natural radiative forcing. In: *Climate Change 2013: The Physical Science Basis. Contribution of Working Group I to the Fifth Assessment Report of the Intergovernmental Panel on Climate Change*. Stocker, TF, Qin D, Plattner G-K *et al.* (eds), Cambridge, UK: Cambridge University Press, 2013.
73. Stuecker MF, Bitz CM, Armour KC *et al.* Polar amplification dominated by local forcing and feedbacks. *Nature Clim Change* 2018;**8**:1076–81.

74. MacMartin DG, Kravitz B. The engineering of climate engineering. *Annu Rev Control Robot Auton Syst* 2019;**2**:445–67.
75. Zhang B, Zhao M, He H *et al.* The dependence of climate sensitivity on the meridional distribution of radiative forcing. *Geophys Res Lett* 2023;**50**(18):e2023GL105492. https://doi.org/10.1029/2023GL105492.
76. Ali H, Mishra V. Contrasting response of rainfall extremes to increase in surface air and dewpoint temperatures at urban locations in India. *Sci Rep* 2017;**7**:1228.
77. Pinto I, Jack C, Lennard C *et al.* Africa's climate response to solar radiation management with stratospheric aerosol. *Geophys Res Lett* 2020;**47**(2):e2019GL086047. https://doi.org/10.1029/2019GL086047.
78. Tilmes S, MacMartin DG, Lenaerts JTM *et al.* Reaching 1.5 and 2.0 °C global surface temperature targets using stratospheric aerosol geoengineering. *Earth Syst Dynam* 2020;**11**:579–601.
79. Bala G, Caldeira K, Nemani R. Fast versus slow response in climate change: implications for the global hydrological cycle. *Clim Dyn* 2010;**35**:423–34.
80. Dinh T, Fueglistaler S. Mechanism of fast atmospheric energetic equilibration following radiative forcing by CO_2. *J Adv Model Earth Syst* 2017;**9**:2468–82.
81. Ferraro AJ, Highwood EJ, Charlton-Perez AJ. Weakened tropical circulation and reduced precipitation in response to geoengineering. *Environ Res Lett* 2014;**9**:014001.
82. Berry G, Reeder MJ. Objective identification of the intertropical convergence zone: climatology and trends from the ERA-Interim. *J Clim* 2014;**27**:1894–909.
83. Haywood JM, Jones A, Bellouin N *et al.* Asymmetric forcing from stratospheric aerosols impacts Sahelian rainfall. *Nature Clim Change* 2013;**3**:660–5.
84. Jones A, Haywood JM, Boucher O. Aerosol forcing, climate response and climate sensitivity in the Hadley Centre climate model. *J Geophys Res* 2007;**112**:D20211. https://doi.org/10.1029/2007JD008688.
85. Smyth JE, Russotto RD, Storelvmo T. Thermodynamic and dynamic responses of the hydrological cycle to solar dimming. *Atmos Chem Phys* 2017;**17**:6439–53.
86. Evans S, Dawson E, Ginoux P. Linear relation between shifting ITCZ and dust hemispheric asymmetry. *Geophys Res Lett* 2020;**47**(22):e2020GL090499. https://doi.org/10.1029/2020GL090499.
87. Frierson DMW, Hwang YT. Extratropical influence on ITCZ shifts in slab ocean simulations of global warming. *J Clim* 2012;**25**:720–33.
88. Schneider T, Bischoff T, Haug GH. Migrations and dynamics of the intertropical convergence zone. *Nature* 2014;**513**:45–53.
89. Cheng W, MacMartin DG, Kravitz B *et al.* Changes in Hadley circulation and intertropical convergence zone under strategic stratospheric aerosol geoengineering. *NPJ Clim Atmos Sci* 2022;**5**:32.
90. Donohoe A, Marshall J, Ferreira D *et al.* The relationship between ITCZ location and cross-equatorial atmospheric heat transport: from the seasonal cycle to the last glacial maximum. *J Clim* 2013;**26**:3597–618.
91. Devaraju N, Bala G, Modak A. Effects of large-scale deforestation on precipitation in the monsoon regions: Remote versus local effects. *Proc Natl Acad Sci U S A* 2015;**112**:3257–62.
92. Michael R. Uncertainties and graphing. 2007. http://spiff.rit.edu/classes/phys311/workshops/w2c/slope_uncert.html (January 2024, date last accessed).
93. Joshi M, Shine K, Ponater M *et al.* A comparison of climate response to different radiative forcings in three general circulation models: towards an improved metric of climate change. *Clim Dyn* 2003;**20**:843–54.
94. Kaur H, Bala G, Seshadri AK. Why is climate sensitivity for solar forcing smaller than for an equivalent CO_2 forcing? *J Clim* 2023;**36**:775–89.
95. Harrop BE, Lu J, Liu F *et al.* Sensitivity of the ITCZ location to ocean forcing Via Q-Flux Green's function experiments. *Geophys Res Lett* 2018;**45**(23):13–116. https://doi.org/10.1029/2018GL080772.
96. Kravitz B, MacMartin DG, Tilmes S *et al.* Comparing surface and stratospheric impacts of geoengineering with different SO_2 injection strategies. *Jgr Atmospheres* 2019;**124**:7900–18.
97. Turner AG, Annamalai H. Climate change and the South Asian summer monsoon. *Nature Clim Change* 2012;**2**:587–95.
98. Kumar PV, Bhavani O, Bhaskar S. Spatial and temporal pattern of deficient Indian summer monsoon rainfall (ISMR): impact on Kharif (summer monsoon) food grain production in India. *Int J Biometeorol* 2023;**67**:485–501. https://doi.org/10.1007/s00484-023-02428-0.
99. Ocko IB, Ramaswamy V, Ming Y. Contrasting climate responses to the scattering and absorbing features of anthropogenic aerosol forcings. *J Clim* 2014;**27**:5329–45.
100. Visioni D, MacMartin DG, Kravitz B *et al.* Seasonal injection strategies for stratospheric aerosol geoengineering. *Geophys Res Lett* 2019;**46**:7790–9.
101. Lee WR, MacMartin DG, Visioni D *et al.* High-latitude stratospheric aerosol geoengineering can be more effective if injection is limited to spring. *Geophys Res Lett* 2021;**48**(9):e2021GL092696. https://doi.org/10.1029/2021GL092696.
102. Zhang Y, MacMartin DG, Visioni D *et al.* How large is the design space for stratospheric aerosol geoengineering? *Earth Syst Dynam* 2022;**13**:201–17.
103. Sanap SD, Pandithurai G. The effect of absorbing aerosols on Indian monsoon circulation and rainfall: A review. *Atmos Res* 2015;**164–165**:318–27.
104. Li J, Carlson BE, Yung YL *et al.* Scattering and absorbing aerosols in the climate system. *Nat Rev Earth Environ* 2022;**3**:363–79.

Oxford Open Climate Change, 2024, 4, 1–15
https://doi.org/10.1093/oxfclm/kgae016
Research Article